CORONARY ANGIOGRAPHY

# Coronary Magnetic Resonance Angiography: Technical Developments and Clinical Applications

**Martijn S. Dirksen,[1,\*] Hildo J. Lamb,[1] Joost Doornbos,[1] Jeroen J. Bax,[2] J. Wouter Jukema,[2] and Albert de Roos[1,#]**

[1]Department of Radiology and [2]Department of Cardiology, Leiden University Medical Center, Leiden, The Netherlands

## ABSTRACT

Magnetic resonance angiography (MRA) is a promising method for noninvasive coronary artery imaging. The interesting features of coronary MRA are its non-invasive nature, the absence of ionizing radiation, and the possibility of imaging the coronary arteries without exogenous contrast. Moreover, three-dimensional volume information and tomographic image planes in any direction can be obtained. The current review presents an overview of the recent technical developments of coronary MRA and the potential clinical applications. New MR techniques, such as parallel image acquisition, spiral imaging, steady-state free precession and the introduction of blood pool contrast agents may result in more efficient data acquisition. After implementation of these fast techniques, coronary MRA may be integrated in a comprehensive cardiac exam.

*Key Words:*   Magnetic resonance imaging; Coronary arteries; Magnetic resonance coronary angiography; Review.

## INTRODUCTION

Coronary artery disease remains the greatest health scourge afflicting the industrialized nations (Braunwold, 1988; Heart and Stroke Statistical Update, 2000). Historically, x-ray angiography has been the standard of reference for diagnosing coronary artery disease.

Despite its efficacy, there are small but definite risks associated with this procedure (Krone et al., 1996; Scanlon et al., 1999). Recent developments have illustrated the potential role for less invasive tests to diagnose coronary artery disease, such as magnetic resonance imaging, multi-slice computed tomography, and electron beam tomography. For example, Achenbach

*Correspondence: Martijn S. Dirksen, M.D., Department of Radiology, C2-S, Leiden University Medical Center, Albinusdreef 2, 2333 ZA Leiden, The Netherlands; E-mail: M.S.Dirksen@lumc.nl.
#Reprints: Albert de Roos, M.D., Department of Radiology C2-S, Leiden University Medical Center, Albinusdreef 2, 2333 ZA Leiden, The Netherlands; Fax: +31-71-5248256; E-mail: A.de_Roos@lumc.nl.

et al. were able to identify significant coronary artery stenosis with a sensitivity of 85% and a specificity of 75% using multislice-computed tomography (Achenbach et al., 2001). Comparable results have been reported for electron beam tomography (Achenbach et al., 1998; Schmermund et al., 1998). Probably the most attractive option is coronary magnetic resonance angiography (MRA), due to its widespread clinical availability and the absence of both ionizing radiation and exogenous contrast enhancement. Kim et al. performed a multi-center trial in which coronary magnetic resonance angiography revealed left main or three-vessel disease with a sensitivity of 100% and a specificity of 85% (Kim et al., 2001). Coronary MRA is still undergoing rapid improvement, aimed to increase its accuracy for visualizing the distal coronary artery segments and to reduce the number of uninterpretable images.

Recently, various new coronary MRA techniques have been introduced to improve the data acquisition speed, spatial resolution, and image contrast, thereby allowing for improved coronary artery visualization. The current review presents an overview of recent technical developments and the clinical applications of coronary MRA.

## PART I: CORONARY MRA TECHNICAL DEVELOPMENTS

Coronary MRA has to deal with several trade-offs between acquisition time, spatial resolution, contrast-to-noise ratio, and the urge for cardiac and respiratory motion correction. New technical developments may facilitate these trade-offs.

### Parallel Image Encoding Techniques: Improving Acquisition Speed

Parallel image encoding was designed to improve acquisition speed, and is known under the acronyms SENSE (SENSitivity Encoding) and SMASH (Simultaneous Acquisition of Spatial Harmonics) (Pruessmann et al., 1999; Pruessmann et al., 2001; Sodickson et al., 1999). The combined application of multiple receiver coils and a reduced sampling of k-space allows for the improved acquisition speed.

In parallel imaging techniques such as SENSE, multiple coil elements are used to simultaneously obtain signal, from the same region. A coil sensitivity map is acquired during a prescan. Each coil has a known specific sensitivity, which is used to calculate the share of each coil in the signal of the acquired anatomical region.

The distance between the individual k-lines is increased and the number of sampling lines is reduced (Fig. 1). Consequently, k-space basically is undersampled, resulting in back-folding effects. Using the spatial and sensitivity encoded information, the back-folded image is reconstructed to an unfolded image using linear algebra. Parallel image encoding can be combined with common coronary MRA approaches like gradient echo and echo planar imaging. Potential disadvantages of parallel image encoding are the extended computation power, the requirement for prescanning (to create the sensitivity map), the signal-to-noise penalty that comes with this technique, and potential inaccuracies in reconstruction (Kurihara et al., 2001; Pruessmann et al., 1999).

Initial experiments with SENSE have shown the potential use for real-time cardiac imaging, by reducing the acquisition time per image down to 27 msec at 2.6 mm resolution (Weiger et al., 2000). For coronary MRA the clinical experiences with parallel imaging are scarce. In preliminary work, Hong et al. demonstrated the feasibility of parallel imaging for coronary MRA and were able to cut down the acquisition time by half when using three-dimensional coronary MRA combined with respiratory navigator motion correction and SENSE as compared to a conventional approach (Hong et al., 2002).

In summary, the main rationale for the application of parallel-image encoding techniques is the improved data acquisition speed, which in turn may allow to obtain higher spatial resolution, lower temporal resolution, or larger three-dimensional volumes. The clinical use of parallel-image encoding techniques needs to be further determined.
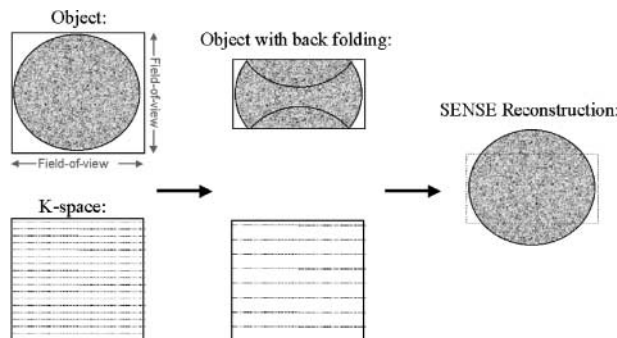


***Figure 1.*** SENSE acquisition. In SENSE imaging, the number of sampling k lines is reduced, which results in back folding effects. With the use of multiple receiver coils, the back folding is spatially encoded and can be reconstructed, using linear algebra, to an unfolded image.

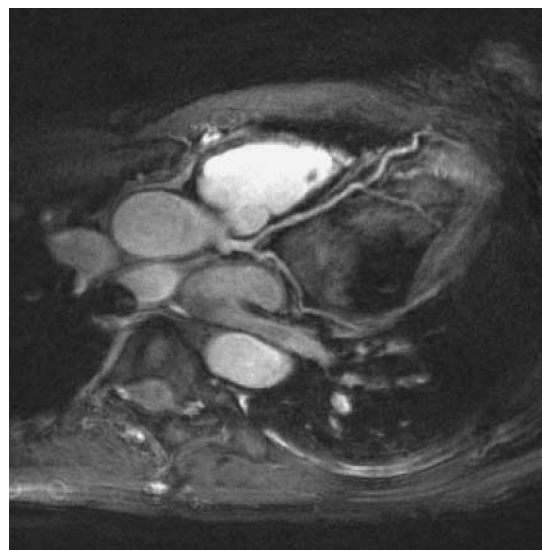## Spiral Coronary MRA: Improving Acquisition Speed

Spiral coronary MRA is a way to improve the image acquisition speed. In spiral acquisition schemes, k-space is sampled more efficiently than in conventional cartesian sampling schemes (Meyer et al., 1992). Spiral k-space sampling has a number of advantages: (a) the acquisition time is reduced, due to the efficient sampling pattern; (b) the image contrast is improved, because sampling is started from the center of k-space, and (c) the acquisitions are relatively insensitive to flow artifacts (Börnert et al., 2001). There are some drawbacks: (a) spiral coronary MRA has a short acquisition duration which may negatively impact the signal-to-noise; (b) spiral coronary MRA is not implemented on clinical systems yet, which hampers clinical evaluation; and (c) spiral coronary MRA is sensitive to main field inhomogeneities that may cause blurring of the images. To solve this potential problem, a field map can be acquired to quantify the off-resonance effects. Then a so-called conjugate phase reconstruction can be performed to reverse the undesired effect. However, a good main field shim over the region of interest is the most important condition to prevent off-resonance effects (Börnert et al., 2001).

Preliminary experiments have been performed by Börnert, Aldefeld, and Nehrke, who proposed a spiral coronary MRA pulse sequence combined with fat saturation, T2 preparation, regional presaturation slabs, and respiratory navigator gating, thereby illustrating the feasibility of spiral data acquisition for coronary MRA (Fig. 2) (Börnert et al., 2001). To date, no clinical data have been reported for the detection of coronary artery stenosis using spiral data acquisition.

## Steady State Free Precession: Improving Image Contrast

Steady-State Free Precession (SSFP) is known under the acronyms FISP, True-FISP (Fast Imaging with Steady-state free Precession, balanced FFE (balanced Fast Field Echo), and FIESTA (Fast Imaging Employing STeady-state Acquisition). SSFP was originally applied to enhance the signal from long T2* components such as fluids in brain imaging, but turned out to provide excellent contrast between blood and myocardium as well (Fig. 3) (Barkhausen et al., 2001; Oppelt et al., 1986; Thiele et al., 2001).

SSFP is characterized by an alternating phase of the excitation pulse combined with the application of time-balanced gradients for all gradient directions: slice selection, frequency, and phase encoding. SSFP obtains the FID as well as the stimulated echo. The practical application of SSFP is enabled by modern MR systems that allow short repetition times and short echo times. SSFP provides high signal intensity for tissues with a high T2/T1 ratio (e.g., blood), with a relative independency of the repetition time and flow artifacts. The SSFP sequence however, is sensitive to field



*Figure 2.* Spiral coronary MRA showing the left coronary artery tree using a magnetization-prepared double interleave three dimensional spiral coronary MRA acquisition (reformatted image). (Courtesy Dr. P. Börnert, Philips Research Laboratories Hamburg, Germany.)



*Figure 3.* Conventional gradient echo vs. steady state free precession. (A) Coronary MRA of the right coronary artery of a healthy volunteer using a 3D gradient echo sequence (TR 7.3 ms, TE 2.0 ms, flip 30°, T2 preparation, respiratory navigator gating, reconstructed resolution 0.53 × 0.53 × 1.5 mm). (B) Same subject, using steady state free precession (TR 5.3 ms, TE 2.7 ms, flip 100°, other parameters identical). The application of steady state free precession results in improved vessel depiction.

inhomogeneities, which makes field shimming an important issue.

SSFP is of special interest for cardiac function analysis. In two studies, SSFP was compared to gradient-echo imaging, and improved endocardial border delineation was reported for the SSFP images, which facilitated automated edge detection during cardiac function analysis (Plein et al., 2001; Thiele et al., 2001). The potential use of SSFP for coronary MRA has recently been shown by Deshpande et al. in a study comparing conventional FLASH (fast low-angle shot) to three-dimensional true-FISP. The signal-to-noise and contrast-to-noise were improved with 55% and 178% respectively for the SSFP acquisitions (Deshpande et al., 2001). In a later preliminary study, Shea et al., showed further contrast improvement with the application of a T2-preparation prepulse in the SSFP sequence (Shea et al., 2002). McCarthy et al. used SSFP for the evaluation of coronary artery stenosis in 17 patients, with x-ray angiography as standard of reference (McCarthy et al., 2001). In this preliminary work, hemodynamically significant stenoses could be detected with a sensitivity of 70% and a specificity of 88%.

At this stage, clinical trials with greater numbers of subjects should be performed to establish SSFP as a diagnostic tool for coronary artery disease.

### Contrast Agents: Improving Image Contrast

Contrast media change the T1 and/or T2 relaxivity of the blood pool. A variety of contrast media is available for coronary MRA. Conventional extravascular (extracellular) contrast media easily diffuse across the fenestrations of the capillary endothelium due to the small molecular size, causing local myocardial signal enhancement and a decrease of the contrast between the coronary arteries and the myocardium, which makes them less useful for coronary MRA. New contrast agents have been developed that exclusively remain in the circulation without the extravasation effects (blood pool agents or intravascular agents), for example P792 (Vistarem®, Guerbet Research, France) (Fig. 4). To prevent extravasation, blood pool agents (BPA) either rely on macromolecular properties or on binding affinity to serum proteins. USPIO agents (ultra small particles of iron oxide) are super-paramagnetic macromolecular compounds with a low r1/r2 relaxivity ratio, and increase the signal intensity of blood only at low concentrations (NC100150, Nycomed Amersham, Oslo, Noway) (Taylor et al., 1999). An example of a protein binding BPA is MS-325 (Epix Medical Inc., Cambridge, MA, USA), which is
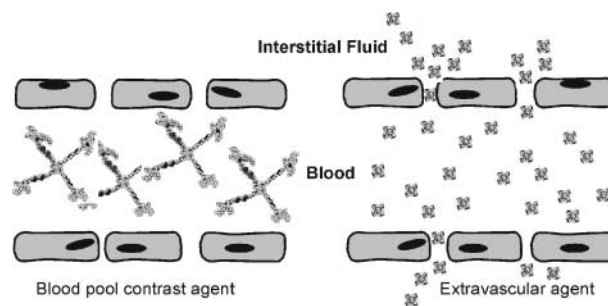


*Figure 4.* Blood pool agents versus extravascular contrast agents. On the left panel, a macromolecular blood pool agent is shown. The molecules are too big to pass the capillary fenestrations and are therefore contained in the circulation. Other blood pool agents may act in a similar way by binding to serum proteins. The left panel shows a conventional small-molecular agent that easily diffuses through the cappilary fenestrations.

a gadolinium compound with reversible binding affinity to serum albumin (Grist et al., 1998; Stuber et al., 1999). Gadolinium compounds predominantly induce T1 effects.

Blood pool agents have particular advantages such as intravascular containment, the relatively high relaxivity properties, and the plasma levels that are maintained for an extended period of time, which allow for coronary MRA acquisitions with relatively long imaging times such as respiratory navigator or multiple breath holds. A potential disadvantage of BPA is that once injected, they may remain in the circulation for hours or even days. Blood pool agents with rapid clearance properties have been developed to allow for acquisition schemes that require multiple bolus injections, such as first-pass contrast enhanced coronary MRA and rest-stress myocardial perfusion imaging. Examples of rapid clearance BPA are P792 and Gadomer-17 (Schering, Berlin, Germany) (Dirksen et al., 2001; Li et al., 2001; Misselwitz et al., 2001; Port et al., 2001).

Recapitulating, blood pool agents, as compared with conventional agents, have specific utility for coronary MRA because of the intravascular distribution and steady plasma levels. The use of blood pool agents combined with new acquisition techniques such as spiral imaging needs to be determined.

### Field Strength >1.5 Tesla: Improving Signal-to-Noise Ratio

Coronary MRA using a static magnetic field strength of 3 Tesla improves the signal-to-noise ratio, which in

turn can be employed to increase the in-plane resolution, reduce the slice thickness, reduce the overall acquisition time, or to compensate for the signal-to-noise penalty that comes with several fast acquisition techniques such as echo planar imaging (EPI) or spiral imaging due to high sampling bandwidths (Dougherty et al., 2001; Wen et al., 1997).

The relation between field-strength and signal-to-noise depends on several factors such as T1 and repetition time. The signal-to-noise ratio follows a squarerootlike function, resulting in smaller gains as the field strength increases (Rinck, 1993). The increased field strength may cause various side effects, especially when subjects move through the static field when entering the bore of the magnet. Side effects such as vertigo or nausea have been mentioned in preliminary reports (Redington et al., 1988).

At this stage, only limited data are available on coronary MRA on 3 Tesla. Preliminary experiments have been performed by Stuber et al. who performed coronary MRA at 3 Tesla using a three-dimensional segmented k-space gradient-echo sequence with respiratory navigator, thereby illustrating the feasibility of 3 Tesla coronary data acquisition (Fig. 5) (Stuber et al., 2002).



*Figure 5.* Clinical example of coronary MRA at 3 Tesla. Coronary MRA was performed on a 3 Tesla Philips MR scanner (Philips Medical Systems, Best, The Netherlands) using a three-dimensional segmented k-space gradient echo TFE sequence with respiratory navigator. A three-dimensional reformat was applied to visualize extensive portions of the left coronary artery tree (Stuber et al., 2002) (Courtesy Dr. M. Stuber, Beth Israel Deaconess Medical Center, Boston).

## Real-Time Data Acquisition

Continuous image acquisition at high frame rates provides improved insight into cardiac dynamics. For coronary MRA, real-time imaging may serve as a localizer for high-resolution coronary MRA acquisitions (Hardy et al., 1998), or for direct coronary visualization. The practical advantages are that real-time imaging operates irrespective of respiratory motion and cardiac arrhythmias.

Data acquisition techniques such as wavelet encoding, sliding reconstruction windows, and echo planar imaging have speeded up the data acquisition, thereby allowing for frame rates even up to 75 msec at 2.5 mm resolution (Chapman et al., 1987; Kerr et al., 1998; McKinnon, 1993; Panych et al., 1993; Riederer et al., 1988; Rzedzian and Pykett, 1987; Saini et al., 1989; Stuber et al., 1997). Recently, Weiger, Pruessmann, and Boesiger combined real-time imaging with sensitivity encoding that resulted in a frame rate of 27 msec per image at 2.3 mm resolution (Weiger et al., 2000).

Hardy et al. evaluated real-time interactive data acquisition for coronary arteries with the aid of a hybrid acquisition approach (Hardy et al., 1998). First, real-time interactive imaging localized the optimal oblique imaging plane. Then, a limited number of contiguous two-dimensional slices of the area of interest were acquired using a breath hold-based segmented gradient echo. In a later report, Hardy illustrated the feasibility of real-time coronary MRA with adaptive averaging in volunteers and concluded real-time coronary MRA to be a robust technique without the need for breath holding, navigation, or electrocardiographic (ECG) gating (Hardy et al., 2000). Potential future applications of real-time imaging include cardiac intervention procedures such as the placement of intracoronary stents, as recently demonstrated by Spuentrup in an animal model (Spuentrup et al., 2002).

## Cardiac Motion Correction; Optimization of the Acquisition Window

Cardiac motion occurs in both systole and diastole, but is said to be minimal in mid-diastole (at diastasis). Cardiac motion correction is therefore usually achieved by timing the acquisition to the mid-diastolic phase of the cardiac cycle.

The contraction of the heart is not symmetrically distributed over the various areas of the cardiac muscle, which causes the coronary artery segments to be subject to different rates of motion, depending on their anatomical

location. Wang, Vidan, and Bergman measured coronary artery motion using dynamic x-ray angiography in 13 patients (Wang et al., 1999). They concluded that there is considerable variation of motion patterns, motion ranges and motion velocities among individual patients. The diastolic rest-period varied from 66 to 333 msec for the left coronary artery and from 66 to 200 msec for the right coronary artery. The rest period was strongly heart-rate dependent. At heart rates higher than 65 beats per minute, the rest periods for the left and the right coronary arteries became equally short, approaching 66 msec. On average, the right coronary artery had greater movement and greater velocity as compared with the coronary artery, up to a factor of two for the proximal segments. An important finding of this study was that the coronary arteries returned to the same location from heartbeat to heartbeat during the rest period, which is an absolute requirement to perform coronary MRA.

The optimal time delay between the electrocardiographic trigger point (the R-wave of the QRS complex) and the acquisition window can be determined in various ways. Several studies have empirically determined the mid-diastolic period in the cardiac cycle using data from heart sound recording, carotid arterial pulse tracing, electrocardiography, and multiphase gradient-echo breath hold MRI (Lewis et al., 1977; Stuber et al., 1999; Weissler et al., 1968). Stuber et al. proposed to calculate the trigger delay (Td) according to the following formula: $Td = [(t_{RR} - 350) \times 0.3] + 350$. In this formula, $tRR = 60/(\text{heart rate})$, which refers to the time delay between two R waves. This formula is based on the assumption that the systolic part of the cardiac cycle has a relatively constant duration of $\sim 350$ msec (Staffeld et al., 1978; Stuber et al., 1999). In a later study, Wang et al. recommended to perform a pre-scan prior to the actual coronary MRA acquisition for the estimation of the electrocardiographic trigger delay of each patient. Wang used an electrocardiographically triggered continuous navigator echo acquisition targeted on the heart, to identify the period of minimal cardiac motion in the cardiac cycle (see Fig. 6) (Wang et al., 2001).

## Vector ECG

The efficacy of ECG sensing during MR acquisitions depends on both the patient and the operator. Imprecise ECG triggering may result from traditional noise sources such as poor electrode contact, lead wire noise, patient movement, muscle contraction, ECG baseline drift, or amplitude modulation due to respiration (Chia et al., 2000). The main interference is caused by a false
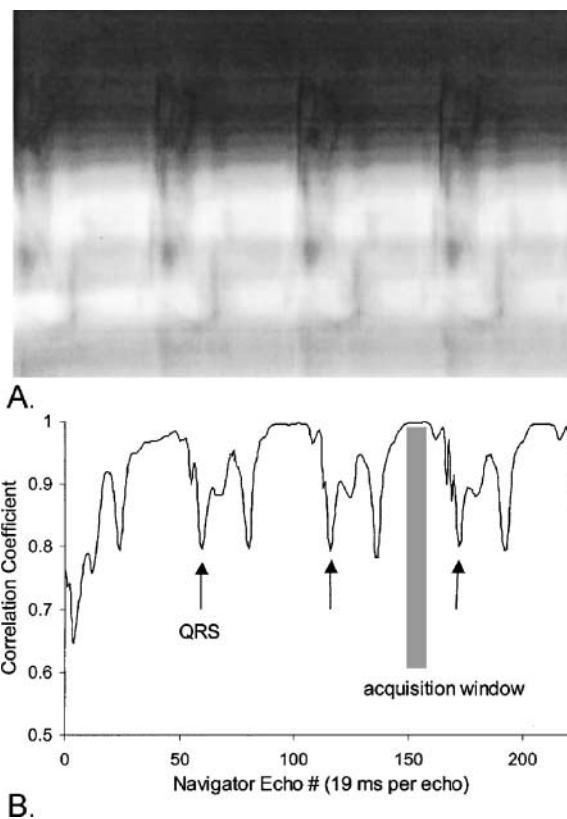


**Figure 6.** Determination of the period of minimal coronary motion using ECG triggered navigator cardiac motion prescanning, from a study performed by Wang et al. The vertical axis is the cranio-caudal direction and the horizontal axis is time. (B) Corresponding correlation graph. The grey bar shows the period of optimal timing. (With permission from the author) (Wang et al., 2001).

triggering on the ST segment instead of the R-wave due to the magnetohydrodynamic effect that results from the magnetic field and induces voltages that superimpose the ST-segment voltage. The rise of the ST segment eventually results in false triggering of the T-wave in favor of the R-wave (Fig. 7). In contrast to conventional scalar ECG, a vector cardiogram system uses multiple ECG channels simultaneously to reconstruct a vector cardiogram, in which the QRS loop is spatially separated from the MR related artifacts (Steenbeck and Pruessmann, 2001). A three-dimensional orthogonal lead system registers the dipole-resolved cardiac electromotive forces over the cardiac cycle (Chia et al., 2000). The temporal and spatial depolarization information thus obtained is used to create a vector that is used for improved triggering.

MARCEL DEKKER, INC. • 270 MADISON AVENUE • NEW YORK, NY 10016
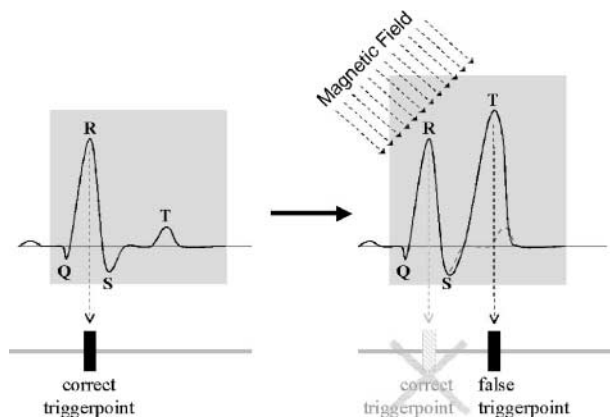
***Figure 7.*** The magneto hydrodynamic effect causes a voltage that superimposes on the ST segments, causing false ECG triggering.

## Respiratory Motion Correction: Navigator and Breath Hold

In addition to the cardiac motion, coronary MRA suffers from artifacts due to respiratory motion. As the heart lies on the diaphragm, it translates during the respiratory cycle in a superoinferior direction. Artifacts caused by respiration movements can be minimized with the aid of several respiratory motion correction approaches. Currently, two major approaches are distinguished: breath holding and free-breathing navigator gating.
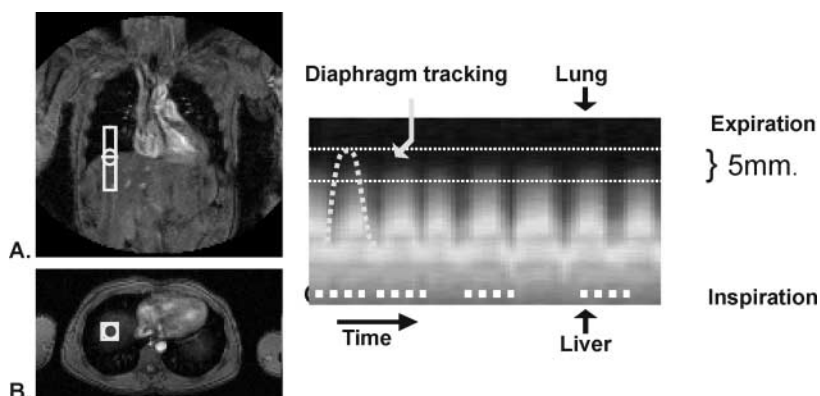
During breath holding, the position of the diaphragm is immobilized and thus the translational shift of the heart. The main limitation of breath holding is

the acquisition time, which is restricted to 10–15 seconds, or even shorter in critically ill patients. Wielopolski et al. has proposed volume coronary angiography using targeted scans (VCATS) to deal with this time restriction (Wielopolski et al., 1998). The VCATS technique relies on a three-dimensional localizer scan that covers the entire heart in a single breath-hold. The three-dimensional information thus obtained is used to determine the optimal planes for high resolution three-dimensional scans that specifically target the coronary segments during breath-hold acquisitions (Fig. 8).

The free-breathing navigator-gating approach is another way to correct for respiratory motion. During navigator gating, the position of the right hemi-diaphragm is deduced in real-time from a navigator pencil beam acquisition (Fig. 9) (Botnar et al., 1999; Stuber et al., 1999). A gating acceptance window is predefined. Image data that are acquired while diaphragm position is within the acceptance window are accepted for filling of the k-space, all other data are discarded. The gating window is chosen at the end-expiratory motion range (Stuber et al., 1999), as this is assumed to be the period of the least diaphragmatic movement. The navigator beam is usually placed on the dome of the right hemi-diaphragm. There are other anatomical interfaces to place the navigator beam on, including the base of the heart. Experiments performed by Stuber et al. showed that placement of the navigator beam on the base of the left ventricular wall has no advantages as compared with navigator placement on the right hemi-diaphragm (Stuber et al., 1999). For the timing of the navigator, Spuentrup et al. concluded that for high resolution submillimeter coronary MRA the acquisition of the navigator beam should be as close to
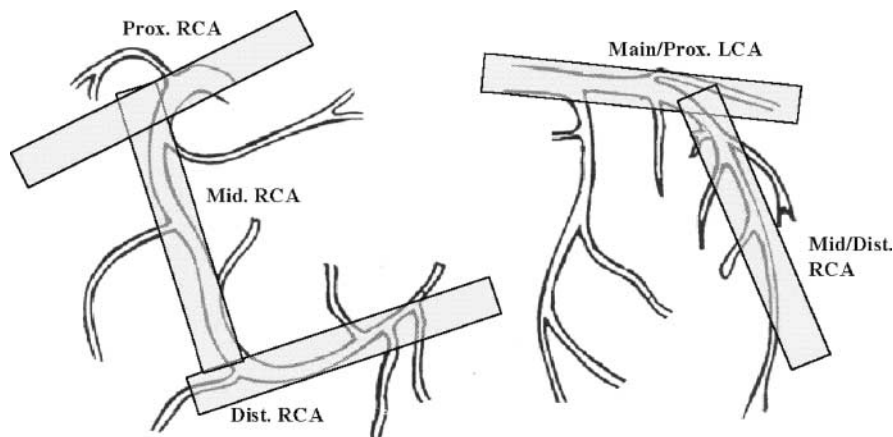


***Figure 8.*** Volume coronary angiography using targeted scans (VCATS). The coronary artery tree is imaged in multiple segments, each acquired with a separate breath-hold.

***Figure 9.*** Respiratory navigator motion compensation. During the coronary MRA image acquisition, a pencil beam echo registrates the position of the diaphragm. Data for the coronary MRA acquisition are only included during the end of expiration. (A) Coronal view of navigator pencil beam and (B) transversal view. (C) Illustrates the diaphragm motion in time. Only during the upper motion range of the diaphragm (5 mm.) data are accepted for k-space filling.

the imaging portion of the pulse sequence as possible (Spuentrup et al., 2002).

Navigator gating implies that only a small fraction of the total imaging time is used for actual data acquisition. This causes the overall imaging time to be prolonged, depending on the navigator efficiency: an acquisition that theoretically takes 4 minutes, will take the twice the amount of time with a navigator acquisition efficiency of 50%. The navigator efficiency depends on several factors, including the anatomical location of the navigator beam and the regularity and nature of the patient's breathing pattern. A clear patient instruction and the patient feeling comfortable therefore play an important role in improving the navigator efficiency. In practice, an average navigator efficiency of 40%–60% can easily be obtained, which however may drop down to 20%–30% in patients that have trouble with regular breathing. The efficiency of navigator gating can be extended by the application motion adapted gating (MAG). In this method, the acceptance window of the diaphragm position is more stringent when low spatial frequencies in k-space are acquired, while the acceptance window gets progressively wider for the periphery of k-space (Hong et al., 2002; Weiger et al., 1997). The clinical feasibility of MAG has recently been illustrated by Weber et al. in a study comparing three-dimensional gradient-echo MRA combined with motion-adapted gating to conventional x-ray angiography. The application of motion-adapted gating resulted in good quality images and allowed for diagnosis of coronary artery disease with a sensitivity of 88% and a specificity of 94% (Weber et al., 2002).

A way to optimize the image quality of navigator-gated acquisitions is the use of slice tracking. This method

moves the position of the image slice according to the observed motion of the diaphragm within the constraints of the acceptance window. It has been shown that the superoinferior motion of the coronary arteries is approximately 60% of the superoinferior displacement of the diaphragm (Stuber et al., 1999; Wang et al., 1995). Recently, Huber et al. proposed a hybrid respiratory motion correction approach by adding an initial breath-hold period to a free-breathing navigator acquisition (Huber et al., 2002). During the breath hold, the most important central portion of the k-space is sampled; the remaining k-space data are acquired using a conventional free-breathing navigator method. This combined approach yielded images with increased signal-to-noise ratio and may be a valuable technique for contrast-enhanced (first-pass) coronary MRA.

## Two-Dimensional vs. Three-Dimensional Imaging

Since the early 1990s, two-dimensional coronary MRA techniques have been used to identify coronary artery stenosis (Manning et al., 1993; Pennell et al., 1996; Post et al., 1997). Two-dimensional coronary MRA using breath hold is subject to several limitations such as partial volume effects, poor overall signal-to-noise, misregistration between adjacent slices due to inconsistent breath holding, and a long overall acquisition time. These limitations, particularly the slice misregistration, can be resolved by using multi-slice two-dimensional acquisitions or three-dimensional acquisitions.

Improved hardware and sophisticated pulse sequences have allowed three-dimensional coronary

MRA that acquires a complete volume during a single breath hold (Wielopolski et al., 1998). Three-dimensional data acquisition allows for extended coverage of anatomical structures, improved signal-to-noise ratio, sophisticated k-space sampling schemes, and isotropic spatial resolution. Three-dimensional data acquisition diminishes the operator dependency and allows for a variety of post processing techniques such as maximum intensity projection (MIP), curved multiplanar reformatting (curved-MPR), and volume rendering techniques (van Geuns et al., 2000; Li et al., 2001; Sandstede et al., 1999; Stuber et al., 1999), as described in the Clinical Applications section.

### Black-Blood Techniques

Conventional bright-blood coronary MRA is usually based on gradient-echo sequences with or without exogenous contrast enhancement. Contrast in bright-blood techniques can be improved with the application of various prepulses such as an inversion prepulse, spectral fat-suppression, and T2-preparation (Botnar et al., 1999; Hofman et al., 1999). Black-blood spin-echo coronary MRA offers particular advantages as compared with bright-blood coronary MRA, such as a high contrast-to-noise ratio, reduced susceptibility to turbulent flow allowing improved coronary artery visualization, and reduced artifacts to metallic objects such as sternal wires, intrathoracic clips and CABG markers (Stuber et al., 2001a; Stuber et al., 2001b).

In black-blood imaging, the blood signal is selectively suppressed in favor of the other tissues by using a double-inversion recovery spin-echo sequence. The first preparatory pulse is a 180° nonslice selective pulse that inverts the magnetization, including all of the blood signal. Then, a second 180° (slice selective) pulse reinverts the spins in the image slice but leaves the blood outside the slice inverted (Fayad et al., 2000). After a specific time delay, the blood from the area with inverted spins will have a zero signal, and has moved in to the image plane resulting in a black blood image (Fig. 10). Stuber et al. (2001a) evaluated a three-dimensional fast spin echo acquisition combined with navigator gating for coronary MRA. This resulted in the visualization of the coronary artery tree with 390 to 700 $\mu$m in-plane resolution, within a reasonable 10 minute acquisition time.

Three-dimensional black-blood imaging allows high contrast between the blood pool, the vascular wall, and the perivascular tissues such as fat and myocardium, which can be traded for improved spatial
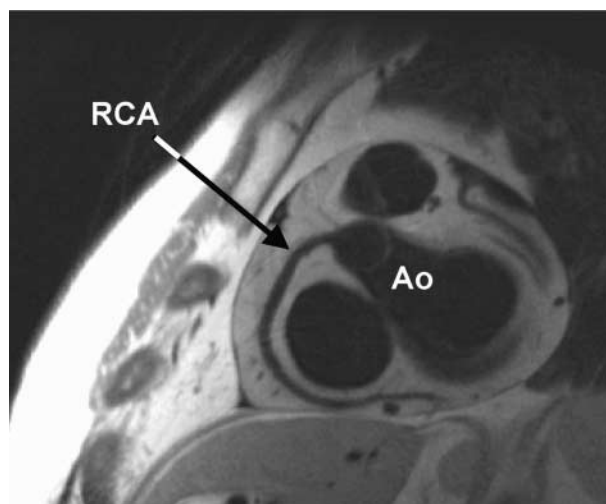


*Figure 10.* Example of black blood imaging of the right coronary artery. RCA = right coronary artery, Ao = Aortic root. (With permission, Dr. M. Stuber, Beth Israel Deaconess Medical Center, Boston.)

resolution (Stuber et al., 2001a). Black-blood imaging therefore has potential application for identification of coronary artery stenosis and for coronary artery lumen measurements (Stuber et al., 2001b). The black-blood imaging sequence reduces blood flow artifacts and motion-related artifacts that are characteristic of nonblack-blood techniques, which can be particularly useful in regions of focal stenosis. Black-blood imaging may result in suboptimal suppression of the blood signal in thick three-dimensional volumes since the concept of dual-inversion black-blood imaging depends on an exchange of the blood pool in the area of interest.

In addition to coronary MRA, another potential application of black-blood imaging techniques is the visualization of the vascular wall and atherosclerotic plaques that cause coronary artery stenosis. Atherosclerotic plaques can be "stable plaques" when consisting of fibrous tissue and calcium. Conversely, the so-called "vulnerable atherosclerotic plaques" consist of a lipid core, covered by a thin fibrous cap, which is prone to rupture, causing intravascular thrombus, which may lead to myocardial infarction. The different kinds of plaques can not be differentiated by conventional x-ray angiography. Recent work by Fayad and Fuster has shown the potential use of magnetic resonance imaging for in vivo plaque characterization (Fayad and Fuster, 2001), which will be discussed more extensively in the clinical sections below.

## PART II: CLINICAL APPLICATIONS OF CORONARY MRA

### Anomalous Coronary Arteries

Anomalous coronary arteries are potentially lethal disorders in a number of cases. Of all adults referred for x-ray angiography because of chest pain, approximately 0.85% turn out to have at least one anomalous coronary artery (Chaitman et al., 1976; Engel et al., 1975; Kimbiris et al., 1978; McConnell et al., 2000). Congenital anomalies like Fallot's Tetralogy are associated with anomalous coronary arteries (Dabizzi et al., 1990). Particularly in children and young adults coronary anomalies are among the main causes of sudden cardiac death (Corrado et al., 1998).

Historically, x-ray angiography has been the standard of reference for diagnosing anomalous coronary arteries, but this technique is hampered by poor spatial information of the course of the coronary arteries in relationship with the great vessels. Coronary MRA allows three-dimensional insight into the origin and course of anomalous coronary arteries, which is an important determinant of eventual clinical events (Ishikawa and Brandt, 1985; Serota et al., 1990). Of all anatomical variants, anomalous coronary arteries that run between the aorta and the pulmonary trunk (intra-arterial) are associated with sudden cardiac death (Fig. 11).

The accuracy of coronary MRA for the identification of anomalous coronary arteries has been demonstrated in several studies (Post et al., 1995). Accurate delineation of the proximal course of coronary anomalies has been shown with sensitivies of 88%–100% and specificies of 100%. In daily practice therefore, coronary MRA may fulfil a significant role in the detection of anomalous coronary arteries, or can be applied whenever x-ray angiography is inconclusive (Post et al., 1995; Taylor et al., 2000; Vliegen et al., 1997).

### Coronary Artery Stenosis

Requirements

The following conditions should be considered for the detection of coronary artery stenosis: (a) The voxel size or interpolated pixel size should be at least smaller than the diameter of the studied vessel. The lumen of coronary arteries typically varies from 4–5 mm in the proximal regions to less than a millimeter in the distal segments. Today, submillimeter spatial resolution is considered a minimum requirement. (b) Adequate cardiac and respiratory motion correction should be achieved, as described previously. (c) The acquisition window duration should be as short as possible to avoid blurring effects due to through-plane motion. (d) The contrast between the coronary artery and the perivascular tissues must allow a clear vessel delineation, which can be achieved by the application of various prepulses, contrast agents, steady-state free precession acquisition techniques, centric k-space sampling, or a combination of these.

Lesion Detection

Lesion detection is usually done by subjective analysis. The observer first decides if specific segments are assessable, according to various classification methods (van Geuns et al., 2000; Kim et al., 2001; Sandstede et al., 1999). The acquisition technique determines how a narrowing is identified (bright blood, black blood, or contrast enhanced). On bright-blood gradient echo images, narrowings are identified by attenuation or absence of the signal intensity, by a narrowing of the arterial lumen, or by signal voids. Signal voids become less prominent with short echo times (Kessler et al., 1999; Sardanelli et al., 2000). Lesion detection on contrast-enhanced acquisitions focuses on the luminal narrowing instead of signal
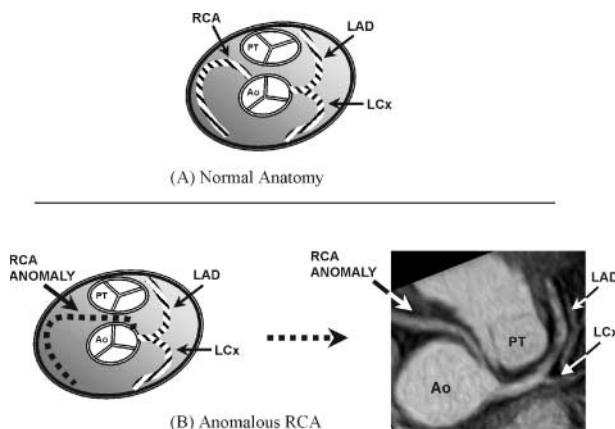
*Figure 11.* Normal and Anomalous right coronary artery. (A) Normal origin and anatomy of the right coronary artery. (B) Anomalous right coronary artery originating from the left coronary sinus. The aberrant RCA courses between aortic root and pulmonary trunk that carries a significant risk of sudden cardiac death. RCA = right coronary artery.

MARCEL DEKKER, INC. • 270 MADISON AVENUE • NEW YORK, NY 10016

voids, as the contrast relies on T1 shortening rather than on flow-related dephasing.

The determination of stenotic lesions may be facilitated with several postprocessing techniques (van Geuns et al., 2000; Li et al., 2001; Sandstede et al., 1999; Stuber et al., 1999). Curved MPR allows for visualization of the tortuous coronary arteries in a single-curved imaging plane, although it depends on the accuracy of the center-line tracking by the operator. Maximum intensity projection projects the bright structures of a three-dimensional volume onto a single imaging plane. Maximum intensity projection may introduce bias concerning stenosis detection, since the proportions of the various signal intensities become distorted. Volume rendering is an excellent postprocessing technique for three-dimensional visualization of the coronary anatomy, and it can show the other cardiac structures at will. Volume rendering adds appreciable time to the overall examination and may yield a greater number of false positives or ignore certain abnormalities, depending on leveling of window and segmentation (van Geuns et al., 2000; Sandstede et al., 1999).

### Two-Dimensional Coronary MRA
### Breath-Hold Approach

With the introduction of the segmented k-space strategies in the early 1990s, coronary MRA became clinically interesting. Several studies have evaluated two-dimensional coronary MRA to detect coronary artery stenosis with varying outcomes, depending on study design and whether proximal or distal segments were evaluated (see Table 1) (Duerinckx, 2001; Manning et al., 1993; Nitatori et al., 1999; Pennell et al., 1996; Post et al., 1997).

### Three-Dimensional Coronary MRA
### Breath-Hold Approach

Three-dimensional coronary MRA combined with breath holding has been evaluated with varying outcomes (van Geuns et al., 2000; Regenfus et al., 2000). Using the VCATS technique as introduced by Wielopolski et al., significant stenosis could be identified with sensitivity of 50% for the LCx (n = 4), 64% for the RCA (n = 14) and 77% for the LM and LAD (n = 13), resulting in an overall sensitivity of 68% and an overall specificity of 97% (see Table 1) (Wielopolski et al., 1998). Figure 12 shows a clinical example of breath-hold based coronary MRA.

### Three-Dimensional Coronary MRA
### Navigator Approach

Three-dimensional coronary MRA combined with respiratory navigator gating has been evaluated in several studies (Huber et al., 1999; Kessler et al., 1997; Kim et al., 2001; Sandstede et al., 1999; Sardanelli et al., 2000; Woodard et al., 1998). For example, Huber et al correctly identified coronary artery stenosis with a sensitivity of 75% for the left main, 62%–71% for the proximal and middle segments of the LAD (depending on image quality subsets), 67%–80% for the proximal and middle LCx, and 86–89% for the proximal and middle segments of the RCA (Huber et al., 1999). In a later study, Sandstede et al. correctly identified coronary stenosis with an overall sensitivity of 81% and an overall specificity of 89% (Sandstede et al., 1999). Figure 13 shows a clinical example of coronary MRA combined with navigator gating.

The clinical utility of 3D navigator coronary MRA was recently evaluated in a multi center trial, performed by Kim et al. (Kim et al., 2001). One hundred nine patients from seven participating centers were enrolled from June 1999 until October 2000. All subjects underwent coronary MRA and conventional x-ray coronary angiography as the standard of reference. The sensitivities for coronary MRA to correctly identify significant stenosis ($\geq 50\%$) were 67% for the left main; 88% for the LAD; 53% for the LCx, and 93% for the RCA. The specificities were respectively 90%, 52%, 70% and 72%. The identification of left main or three-vessel disease could be performed with 100% sensitivity and 85% specificity. This study shows that three-dimensional coronary MRA allows for accurate detection of coronary artery disease in multiple cardiovascular research centers and constitutes a major progression in the development of noninvasive detection of coronary artery disease.

### Contrast-Enhanced Approach

Contrast agents, particularly blood pool agents, can be useful for coronary MRA. Most blood agents are currently under clinical trial evaluation and are expected to become available for clinical use on the short-term. Some potential indications are: (a) anomalous coronary arteries detection, (b) coronary artery stenosis detection and the visualization of collateral flow, (c) coronary bypass graft imaging, and (d) the assessment of relative perfusion and vascular integrity (Saeed et al., 2000).

***Table 1.***  Sensitivity and specificity for detection of coronary artery stenosis by coronary MRA; a selected overview of the literature.

| | # Pat. | # Les. | Sensitivity | | Specificity | |
|---|---|---|---|---|---|---|
| **2D Approach** | | | | | | |
| Manning et al. 1993 (Manning et al., 1993) | 39 | 52 | 90% | (LM 100%, LAD 87%, LCx 71%, RCA 100%) | 92% | (LM 100%, LAD 92%, LCx 90%, RCA 78%) |
| Post et al. 1997 (Post et al., 1997) | 35 | 35 | n.a. | (LM 100%, LAD 53%, LCx 0%, RCA 71%)[a] | n.a. | LM 93%, LAD 73%, LCx 96%, RCA 82%)[a] |
| Pennell et al. 1996 (Pennell et al., 1996) | 39 | 55 | 85 | (LAD 88%; RCA 75-100%; LCx 75%)[b] | n.a. | |
| **3D Breath-hold approach** | | | | | | |
| van Geuns et al. 2000 (van Geuns et al., 2000) | 38 | 31 | 68% | (LM & LAD 77%; LCx 50%; RCA 64%) | 97% | (LM & LAD 97%; LCx 100%; RCA 94%) |
| **Contrast enhanced 3D breath-hold approach** | | | | | | |
| Regenfus et al. 2000 (Regenfus et al., 2000) | 50 | 56 | 94% | (Overall result)[d] | 57% | (Overall result)[d] |
| **3D navigator Approach** | | | | | | |
| Woodard et al. 1997 (Woodard et al., 1998) | 10 | 10 | 70–73% | (Overall result) | n.a. | |
| Kessler et al. 1997 (Kessler et al., 1997) | 73 | 43 | 65% | (Overall result) | 88% | (Overall result) |
| Huber et al. 1998 (Huber et al., 1999) | 20 | 53 | 73–79%[c] | (LM 75%; LAD 62–71%; RCA 86–89%; LCx 67–80%)[c] | 50–54%[c] | LM 25–36%; LAD 46–50%; RCA 67–69%; LCx 58–63%)[c] |
| Sandstede et al. 1999 (Sandstede et al., 1999) | 30 | 37 | 81% | (Overall result) | 89% | (Overall result) |
| Sardanelli et al. 2000 (Sardanelli et al., 2000) | 42 | 67 | 82% | Prox. segments (<5 cm) 90%; dist. segments (>5 cm) 68% | 89% | Prox. Segments (<5 cm) 90%; dist. segments (<5 cm) 81% |
| Kim et al. 2001 (Kim et al., 2001) | 109 | 94 | n.a. | (LM 67%; LAD 88%, LCx 53%, RCA 93%)[e] | n.a. | (LM 90%; LAD 52%; LCx 70%; RCA 72%)[e] |

Pat. = Patients; Les. = Lesions; LM = Left main coronary artery; LAD = Left anterior descending artery; LCx = Left circumflex artery; RCA = Right coronary artery.
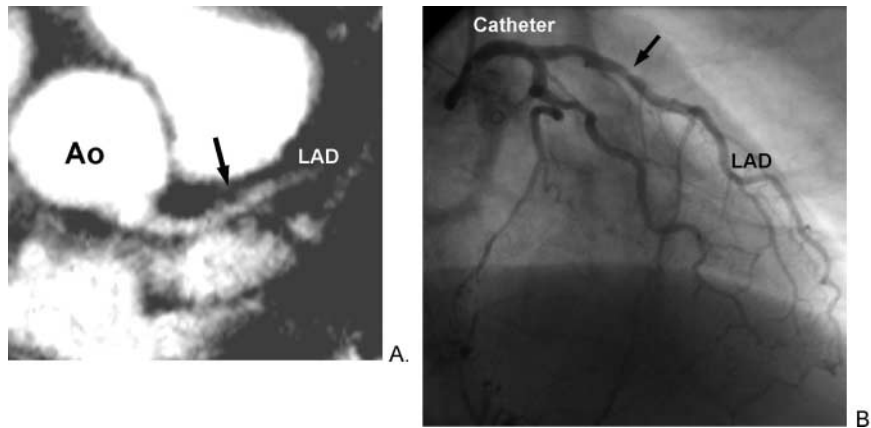[a] Depending on confidence level; sensitivity & specificity for 'possible stenosis'.
[b] Study interpretation not fully blinded.
[c] depending on image quality subsets.
[d] Calculated on a patient-basis instead of segment-basis.
[e] Results from multiple study centers.

MARCEL DEKKER, INC. • 270 MADISON AVENUE • NEW YORK, NY 10016

***Figure 12.*** Example of a focal stenosis of the left coronary artery. (A) Image acquired using a gradient echo coronary MRA approach during a single breath-hold, combined T2-preparation for suppression of the myocardial tissues. (B) Corresponding x-ray angiography. The black arrow indicates the stenosis on the MRA image and on the corresponding x-ray angiography. A0 = aorta, LAD = left anterior descending artery.

The application of extravascular contrast agents for coronary MRA has been evaluated by Li et al. and Deshpande et al., who illustrated increased signal-to-noise ratio, contrast-to-noise ratio, visualized vessel length, and vessel sharpness as compared with noncontrast enhanced techniques (Deshpande et al., 2001; Li et al., 2001). Kessler et al. evaluated an extravascular agent for identification of coronary artery stenosis using three-dimensional breath hold-based coronary MRA, resulting in correct identification of 47 out of 52 coronary arteries and three out of five significant stenoses (Kessler et al., 1999). Regenfus et al. evaluated a cohort of 50 patients with suspected coronary artery disease, using a three-dimensional single breath-hold method combined with an extravascular contrast agent. On a patient basis, coronary artery stenosis could be identified with a sensitivity of 94% and a specificity of 57% (Regenfus et al., 2000). Preliminary studies show that blood-pool agents have the potential to improve the contrast between the coronary arteries and the perivascular tissues (Fig. 14) (Dirksen et al., 2001; Hofman et al., 1999; Li et al., 1998; Li et al., 2001; Stuber et al., 1999). Although there is promising application for BPA, clinical trials need to be performed to evaluate BPA for the detection of coronary artery stenosis.

In conclusion, today's techniques for three-dimensional coronary MRA are able to provide excellent
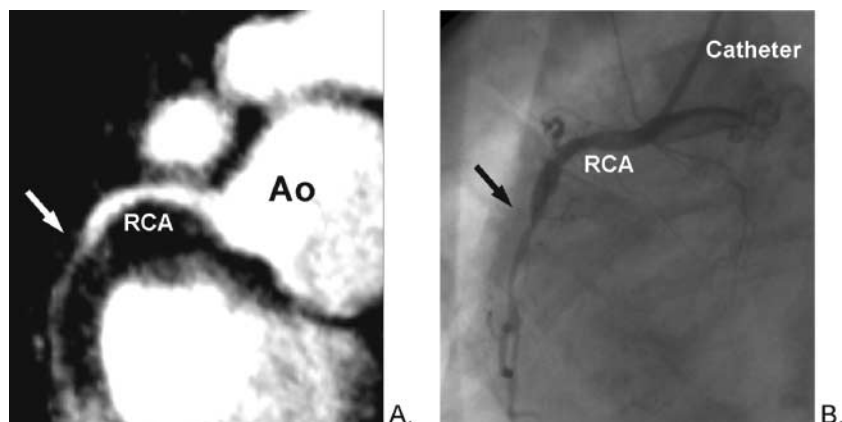


***Figure 13.*** Example of a right coronary artery stenosis. (A) Image acquired using a gradient echo coronary MRA approach combined with navigator and T2 preparation (multi planar reformat). The stenotic area is indicated by a white arrow on the MRA image and by a black arrow on the corresponding x-ray angiography image (B). Ao = aorta, RCA = right coronary artery.
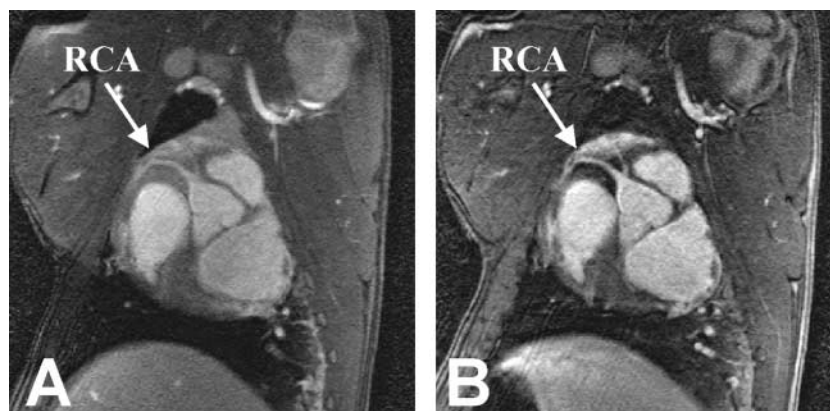
**Figure 14.** A blood pool contrast agent may help to improve coronary artery depiction. (A) Gradient echo technique combined with navigator and T2-preparation of the right coronary artery without exogenous contrast; repetition time 7.1 ms, echo-time 1.9 ms, flip angle 30°; 0.70 × 1.01 × 1.5 mm resolution. The acquisition duration was 49.8 ms in diastole. (B) Identical acquisition, using a blood pool contrast agent and a suppression prepulse whereas the T2 preparation was omitted, resulting in improved vessel depiction (results from an animal experiment). RCA = right coronary artery.

high-resolution images. However, MRA is still hampered by poor sensitivity and specificity for diagnosing coronary artery disease in distal segments. With recent studies, such as the multicenter study performed by Kim et al., it is becoming clear that coronary MRA, under the condition. of persistently accurate study results, may identify or rule out proximal coronary artery disease in a noninvasive way. For the detection of more distally oriented stenoses, coronary MRA still needs considerable improvement.

### Vessel Wall and Plaque Imaging

Atherosclerotic plaque formation is the basis of coronary artery disease. An accurate method for vessel wall and plaque imaging may advance our understanding of the etiology of coronary artery disease and may help in selecting the appropriate medical treatments or surgical interventions. Existing imaging methods for coronary imaging such as intravascular ultrasound (IVUS), multi-slice CT, electron beam tomography, and angioscopy yield limited information about plaque composition. Recent studies have illustrated that MRI can noninvasively image the arterial wall and evaluate atherosclerotic plaques in the aorta and carotid arteries (Fayad et al., 2000; Hatsukami et al., 2000; Toussaint et al., 1996). Fayad et al. have illustrated the potential use of black-blood MRA to visualize the coronary artery wall and were able to show wall-thickening in diseased coronary arteries, but at the same time they pointed out that further studies are required for in vivo characterization of
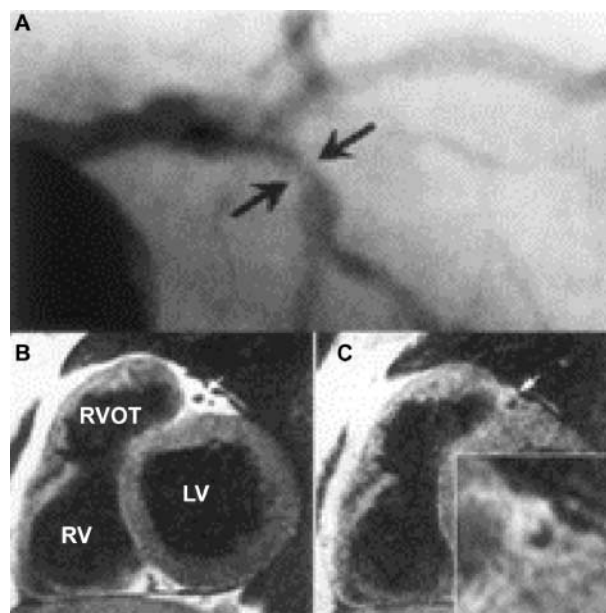


**Figure 15.** Example of vessel wall and plaque imaging using black-blood coronary MRA, with the corresponding angiogram. (A) The x-ray angiogram shows a high-grade stenosis in the proximal segment of the left anterior descending artery (LAD) (black arrows). (B) Cross-sectional black-blood image of the LAD lumen shows an elliptical lumen shape, indicating obstructive disease. (C) Wall image showing a large eccentric plaque with heterogeneous signal intensity. RVOT = right ventricular outflow tract; RV = right ventricle; LV = left ventricle. (Courtesy Dr. Fayad, Mount Sinai School of Medicine, New York.)

coronary plaque composition (Fig. 15) (Fayad et al., 2000). The use of contrast agents has recently been discussed for plaque visualization by Ruehm et al. In an animal experiment they showed that ultra small superparamagnetic iron oxide (USPIO) contrast particles are phagocytozed by macrophages and thus accumulate in aortic atherosclerotic plaques causing marked susceptibility effects and may therefore act as atherosclerotic plaque marker (Ruehm et al., 2001).

Currently, spatial resolution is a limitation for MRI to characterize coronary atherosclerotic plaque. However, the continuous improvements of software and hardware make MR vessel wall and plaque imaging a very promising imaging modality with potential use for diagnosis, treatment, and prevention of atherosclerotic disease.

## Coronary Bypass Graft Imaging

Coronary artery bypass grafting (CABG) is performed in patients that do not adequately respond to medical intervention or wire guided angioplasty. In the United States 1 in every 1000 persons receives a surgical revascularization procedure with an estimated 300,000 operations annually (Gersh et al., 1997). Every patient receiving CABG will soon or later be confronted with the need for a diagnostic test to evaluate the bypass graft patency. Currently, x-ray angiography is the diagnostic procedure of first choice, although it has a small risk of significant complications. Moreover, in the United States, over a million diagnostic x-ray angiograms are performed annually, of which 20% show no significant stenosis (Johnson and Krone, 1993). Therefore, a noninvasive technique, serving as primary screening station, would be of great value.

Since 1987, magnetic resonance imaging has been proposed as a tool to evaluate bypass graft patency, using spin-echo and gradient-echo techniques (Gomes et al., 1987; Rubinstein et al., 1987; White et al., 1987). Several studies followed, with good sensitivity and moderate specificity for the assessment of graft patency (Galjee et al., 1996). The accurate evaluation of graft patency is hampered by several impediments, including motion artifacts, small distal graft size, and metallic clip artifacts.

MR techniques to image bypass grafts are basically the same as those described in the section about coronary artery stenosis. The main differences with coronary MRA is that bypass grafts, especially venous grafts, have larger luminal diameter and a less tortuous course, and therefore are potentially easier to image. Several studies have

shown the accuracy of magnetic resonance angiography for the evaluation of bypass graft patency (Table 2) (Engelmann et al., 2000; Galjee et al., 1996; Langerak et al., 2002; Molinari et al., 2000; Wintersperger et al., 1998). For example, Molinari et al. used a gradient-echo navigator sequence to assess 51 bypasses in 18 patients. In this study, occluded bypass grafts could be identified with 91% sensitivity and 97% specificity with x-ray angiography as reference (Molinari et al., 2000). Engelmann et al. performed gadolinium-enhanced three-dimensional breath-hold MRA to evaluate CABG patency with x-ray angiography as reference. CABG patency could be determined with a sensitivity of 92% for venous grafts and a sensitivity of 100% for internal mammary artery grafts (Engelmann et al., 2000). Vrachliotis et al., used a breath-hold coronary MRA technique combined with an extravascular contrast agent for the assessment of CABG patency. CABG patency could be determined with 93% sensitivity and 97% specificity (Vrachliotis et al., 1997). Recently, Langerak et al. (Langerak et al., 2002) evaluated 56 vein grafts from 38 patients presenting with recurrent chest pain after bypass surgery. A gradient echo MRA technique was combined with navigator gating and T2 preparation to suppress the myocardial tissues, as previously described by Botnar et al. (Botnar et al., 1999). Using this approach, vein graft occlusion could be detected with a sensitivity of 83% and a specificity of 98%–100%. In addition, they showed the diagnostic properties of high resolution three-dimensional MRA ($0.7 \times 1.00 \times 1.50$ mm resolution) in evaluating the severity vein graft stenosis, thereby offering perspective for noninvasive screening of patients with chest pain after bypass surgery (Fig. 16).

In addition to the CABG morphology, the hemodynamic significance of a suspected stenosis may be evaluated with the use of MR flow quantification. Bypass graft flow measurements are based on three observations. (1) A biphasic flow pattern, suggesting normal bypass function (Fig. 17) (Hoogendoorn et al., 1995; Langerak et al., 2001); (2) A flow gradient along the course of a diseased vessel, which provides information on residual CABG function and the severity of stenosis; and (3) The flow reserve, which provides information about bypass graft function.

In 1996, Galjee et al. (Galjee et al., 1996) identified a biphasic flow pattern in 85% of 73 patent grafts using cine-gradient-echo-phase-velocity mapping, illustrating that quantitative flow measurements of bypass grafts are useful for the non-invasive assessment of graft patency and function. Hoogendoorn et al. showed that stenotic grafts, as compared with healthy grafts, showed a flow reduction of 71 ml/min to 9 ml/min using a gradient-echo

**Table 2.** Sensitivity and specificity for the evaluation of bypass graft patency; a selection from the literature between 1987 and 2002.

| | # CABG | MRA technique | Sensitivity | | Specificity | |
|---|---|---|---|---|---|---|
| Rubinstein et al. 1987 (Rubinstein et al., 1987) | 47 | Multislice SE (2D) | 90% | | 72% | |
| White et al. 1988 (White et al., 1988) | 28 | Cine GE (2D) | 93% | (Venous and arterial grafts) | 86% | (Venous and arterial grafts) |
| Aurigemma et al. 1989 (Aurigemma et al., 1989) | 45 | Cine GE (2D) | 88% | (Venous and arterial grafts) | 100% | (Venous and arterial grafts) |
| Galjee et al. 1996 (Galjee et al., 1996) | 98 | SE/cine GE (2D) | 98% | (Only vein grafts) | 85%–88%[a] | (Only vein grafts) |
| Molinari et al. 2000 (Molinari et al., 2000) | 51 | 3D GE & navigator | 91%[b] | (Venous and arterial grafts) | 97%[b] | (Venous and arterial grafts) |
| Engelmann et al. 2000 (Engelmann et al., 2000) | 133 | Contrast enhanced 3D GE & BH | 92%–100% | (92% for venous grafts and 100% for arterial grafts) | 85% | (Only venous grafts) |
| Wintersperger et al. 1998 (Wintersperger et al., 1998) | 76 | Contrast enhanced 3D GE & BH | 95% | (94% for venous grafts and 96% for arterial grafts) | 67–85% | (85% for venous grafts and 67% for arterial graft) |
| Langerak et al. 2002 (Langerak et al., 2002) | 56 | 3D GE & navigator | 83%[b] | (Only vein grafts) | 98–100%[b,c] | (Only vein grafts) |

CABG = coronary artery bypass graft; SE = spin echo; GE = gradient echo; BH = breath hold respiratory motion correction; navigator = navigator respiratory motion correction.

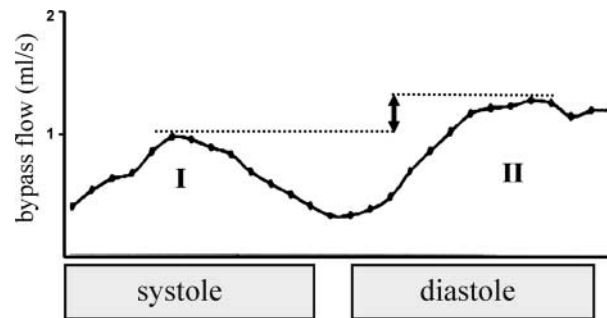[a]Depending on acquisition technique; SE or cine GE.

[b]Sensitivity and specificity for the detection of graft occlusion instead of patency.

[c]Depending on observer.
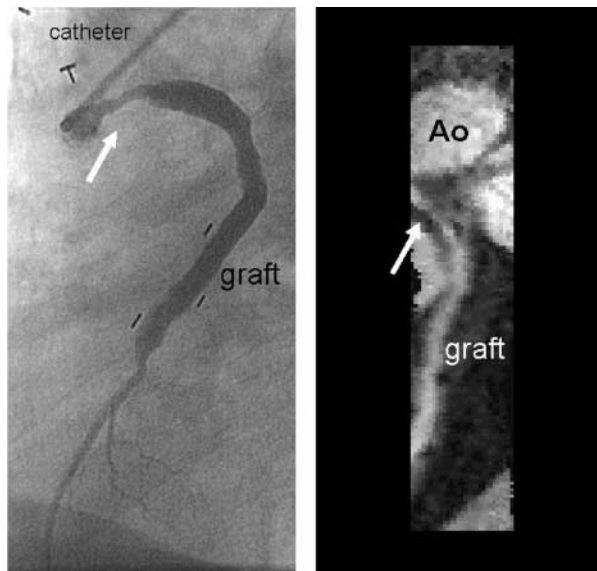
*Figure 16.* Diseased vein graft with proximal stenosis (white arrow) and the corresponding x-ray angiography. (Courtesy S.L. Langerak, Leiden University Medical Center, Leiden, The Netherlands.)



*Figure 17.* Flow rate vs. time in a patient with a venous bypass graft. The biphasic flow pattern can be readily identified, suggesting healthy bypass graft function. (Courtesy S.L. Langerak, Leiden University Medical Center, Leiden, The Netherlands.) (Langerak et al., 2001)

MR technique. A biphasic flow pattern was readily identified in healthy grafts whereas absent in stenotic bypass grafts (Hoogendoorn et al., 1995). Similar results have been reported by Kawada et al. in preliminary work, showing a decrease of CABG flow in diseased bypass grafts as compared with healthy bypass grafts (14 ml/min vs. 76 ml/min) (Kawada et al., 1998). Recently, Langerak et al. evaluated aortic and internal mammary grafts using a fast acquisition technique consisting of turbo-field echo-planar imaging combined with breath holding, which allowed for spatial and temporal resolution of $0.8\,mm^2$ and 23 msec respectively. Conventional cine gradient-echo imaging was used as standard of reference. In this study if 11 subjects with 20 angiographically normal grafts, total CABG blood flow was measured at rest and during adenosine infusion. Good agreements were observed between the conventional gradient echo
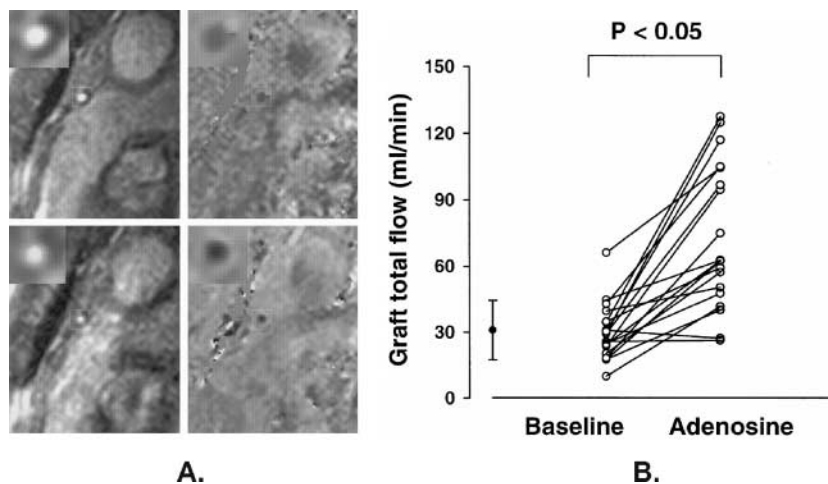


*Figure 18.* Example of MR coronary artery bypass flow measurements. (A) Oblique sagittal modulus (left) and phase flow (right) images of a bypass graft obtained by turbo-field echo-planar imaging at rest (top) and during pharmacological stress (bottom). (B) Corresponding flow measurements of a total of 20 healthy bypass grafts without stenosis at rest and during pharmacological stress. On average, the bypass flow increases in response to the pharmacological stress, indicating normal bypass graft function. (Courtesy S.L. Langerak, Leiden University Medical Center, Leiden, The Netherlands.)

and turbo-field echo-planar techniques for aortic flow (correlation coefficient 0.90) and internal mammary artery flow (correlation coefficient 0.84). Using the turbo-field echo-planar imaging technique, typical biphasic flow and significantly increased flow during pharmacological stress were identified (Fig. 18). This study illustrates the potential use for MRI to determine flow and flow reserve in bypass grafts (Langerak et al., 2001).

The evaluation of coronary bypass graft patency, based on morphology and function, provides important diagnostic information. Clinical trials remain to be performed to validate these results in large patient cohorts.

## CONCLUSIONS

The development of coronary MRA has progressed rapidly. Improvements in imaging techniques such as segmented k-space strategies, fast gradient-echo techniques, or black-blood imaging, have made it possible to consistently visualize proximal and middle segments of the coronary arteries with submillimeter in-plane resolution. Today, coronary MRA is a legitimate indication to detect coronary anomalies and to visualize the three-dimensional course. Diagnosis of coronary artery stenosis is possible with moderate to good accuracy for the proximal and middle segments, but remains a challenging issue for distal segments. Further technical developments such as parallel image acquisition, spiral imaging, steady-state free precession, and the introduction of blood-pool contrast agents allow for a more efficient data acquisition. After implementation of these fast techniques, coronary MRA may be integrated in a comprehensive cardiac exam.

## REFERENCES

Achenbach, S., Moshage, W., Ropers, D., Nossen, J., Daniel, W. G. (1998). Value of electron-beam computed tomography for the noninvasive detection of high-grade coronary-artery stenoses and occlusions. *N. Engl. J. Med.* 339:1964–1971.

Achenbach, S., Giesler, T., Ropers, D., Ulzheimer, S., Derlien, H., Schulte, C., Wenkel, E., Moshage, W., Bautz, W., Daniel, W. G., Kalender, W. A., Baum, U. (2001). Detection of coronary artery stenoses by contrast-enhanced, retrospectively electrocardiographically-gated, multislice spiral computed tomography. *Circulation* 103:2535–2538.

Aurigemma, G. P., Reichek, N., Axel, L., Schiebler, M., Harris, C., Kressel, H. Y. (1989). Noninvasive determination of coronary artery bypass graft patency by cine magnetic resonance imaging. *Circulation* 80:1595–1602.

Börnert, P., Aldefeld, B., Nehrke, K. (2001). Improved 3D spiral imaging for coronary MR angiography. *Magn. Reson. Med.* 45:172–175.

Barkhausen, J., Ruehm, S. G., Goyen, M., Buck, T., Laub, G., Debatin, J. F. (2001). MR evaluation of ventricular function: true fast imaging with steady- state precession versus fast low-angle shot cine MR imaging: feasibility study. *Radiology* 219:264–269.

Botnar, R. M., Stuber, M., Danias, P. G., Kissinger, K. V., Manning, W. J. (1999). Improved coronary artery definition with T2-weighted, free-breathing, three-dimensional coronary MRA. *Circulation* 99:3139–3148.

Braunwold, E. (1988). Heart disease. *A Textbook of Cardiovascular Medicine*. 3rd ed. Philadelphia, USA: W.B. Saunders Company.

Chaitman, B. R., Lesperance, J., Saltiel, J., Bourassa, M. G. (1976). Clinical, angiographic, and hemodynamic findings in patients with anomalous origin of the coronary arteries. *Circulation* 53:122–131.

Chapman, B., Turner, R., Ordidge, R. J., Doyle, M., Cawley, M., Coxon, R., Glover, P., Mansfield, P. (1987). Real-time movie imaging from a single cardiac cycle by NMR. *Magn. Reson. Med.* 5:246–254.

Chia, J. M., Fischer, S. E., Wickline, S. A., Lorenz, C. H. (2000). Performance of QRS detection for cardiac magnetic resonance imaging with a novel vectorcardiographic triggering method. *J. Magn. Reson. Imaging* 12:678–688.

Corrado, D., Basso, C., Schiavon, M., Thiene, G. (1998). Screening for hypertrophic cardiomyopathy in young athletes. *N. Engl. J. Med.* 339:364–369.

Dabizzi, R. P., Teodori, G., Barletta, G. A., Caprioli, G., Baldrighi, G., Baldrighi, V. (1990). Associated coronary and cardiac anomalies in the tetralogy of fallot an angiographic study. *Eur. Heart J.* 11:692–704.

Deshpande, V. S., Shea, S. M., Laub, G., Simonetti, O. P., Finn, J. P., Li, D. (2001). 3D magnetization-prepared true-FISP: a new technique for imaging coronary arteries. *Magn. Reson. Med.* 46:494–502.

Deshpande, V. S., Wielopolski, P. A., Shea, S. M., Carr, J., Zheng, J., Li, D. (2001). Coronary artery imaging using contrast-enhanced 3D segmented EPI. *J. Magn. Reson. Imaging* 13:676–681.

Dirksen, M.S., Lamb, H.J., Kunz, P., Robert, P., Corot, C., de Roos A. (2001). Improved Coronary MRA Using a New Blood Pool Contrast Agent (P-792) and Respiratory Navigator Gating. Proceedings of the International Society of Magnetic Resonace in Medicine 2001, Glasgow, UK, April 21–27, 1854.

Dougherty, L., Connick, T. J., Mizsei, G. (2001). Cardiac imaging at 4 Tesla. *Magn. Reson. Med.* 45:176–178.

Duerinckx, A. J. (2001). Imaging of coronary artery disease. *J. Thorac. Imaging* 16:25–34.

Engel, H. J., Torres, C., Page, H. L. Jr. (1975). Major variations in anatomical origin of the coronary arteries: angiographic

observations in 4,250 patients without associated congenital heart disease. *Cathet. Cardiovasc. Diagn.* 1:157–169.

Engelmann, M. G., Knez, A., von Smekal, A., Wintersperger, B. J., Huehns, T. Y., Hofling, B., Reiser, M. F., Steinbeck, G. (2000). Non-invasive coronary bypass graft imaging after multivessel revascularisation. *Int. J. Cardiol.* 76:65–74.

Fayad, Z. A., Fuster, V. (2001). Clinical imaging of the high-risk or vulnerable atherosclerotic plaque. *Circ. Res.* 89:305–316.

Fayad, Z. A., Fuster, V., Fallon, J. T., Jayasundera, T., Worthley, S. G., Helft, G., Aguinaldo, J. G., Badimon, J. J., Sharma, S. K. (2000). Noninvasive in vivo human coronary artery lumen and wall imaging using black-blood magnetic resonance imaging. *Circulation* 102:506–510.

Fayad, Z. A., Nahar, T., Fallon, J. T., Goldman, M., Aguinaldo, J. G., Badimon, J. J., Shinnar, M., Chesebro, J. H., Fuster, V. (2000). In vivo magnetic resonance evaluation of atherosclerotic plaques in the human thoracic aorta: a comparison with transesophageal echocardiography. *Circulation* 101:2503–2509.

Galjee, M. A., van Rossum, A. C., Doesburg, T., van Eenige, M. J., Visser, C. A. (1996). Value of magnetic resonance imaging in assessing patency and function of coronary artery bypass grafts an angiographically controlled study. *Circulation* 93:660–666.

Gersh, B. J., Braunwald, E., Rutherford, J. D. (1997). Heart disease. In: Braunwald, E., ed. *A Textbook of cardiovascular medicine*. 5th ed. Philadelphia: WB Saunders, p. 1316.

Gomes, A. S., Lois, J. F., Drinkwater, D. C. Jr., Corday, S. R. (1987). Coronary artery bypass grafts: visualization with MR imaging. *Radiology* 162:175–179.

Grist, T. M., Korosec, F. R., Peters, D. C., Witte, S., Walovitch, R. C., Dolan, R. P., Bridson, W. E., Yucel, E. K., Mistretta, C. A. (1998). Steady-state and dynamic MR angiography with MS-325: initial experience in humans. *Radiology* 207:539–544.

Hardy, C. J., Darrow, R. D., Pauly, J. M., Kerr, A. B., Dumoulin, C. L., Hu, B. S., Martin, K. M. (1998). Interactive coronary MRI. *Magn. Reson. Med.* 40:105–111.

Hardy, C. J., Saranathan, M., Zhu, Y., Darrow, R. D. (2000). Coronary angiography by real-time MRI with adaptive averaging. *Magn. Reson. Med.* 44:940–946.

Hatsukami, T. S., Ross, R., Polissar, N. L., Yuan, C. (2000). Visualization of fibrous cap thickness and rupture in human atherosclerotic carotid plaque in vivo with high-resolution magnetic resonance imaging. *Circulation* 102:959–964.

American Heart Association, (2000). *Heart and Stroke Statistical Update*. Dallas, Texas: American Heart Association.

Hofman, M. B., Henson, R. E., Kovacs, S. J., Fischer, S. E., Lauffer, R. B., Adzamli, K., De Becker, J., Wickline, S. A., Lorenz, C. H. (1999). Blood pool agent strongly improves 3D magnetic resonance coronary angiography using an inversion pre-pulse. *Magn. Reson. Med.* 41:360–367.

Hong, S., Muthupillai, R., Smink, J., Flamm, S. D. (2002). Accelerated acquisition of free breathing navigator-guided coronary MR angiography using sensitivity encoding and motion adapted gating (MAG) The society for cardiovascular magnetic resonance. *J. Cardiovasc. Magn. Reson.* 1(128):26, Fifth Annual Scientific Sessions, Florida, USA, Jan 25–27.

Hoogendoorn, L. I., Pattynama, P. M., Buis, B., van der Geest, R. J., van der Wall, E. E., de Roos, A. (1995). Noninvasive evaluation of aortocoronary bypass grafts with magnetic resonance flow mapping. *Am. J. Cardiol.* 75:845–848.

Huber, A., Nikolaou, K., Gonschior, P., Knez, A., Stehling, M., Reiser, M. (1999). Navigator echo-based respiratory gating for three-dimensional MR coronary angiography: results from healthy volunteers and patients with proximal coronary artery stenoses. *AJR Am. J. Roentgenol.* 173:95–101.

Huber, M. E., Oelhafen, M. E., Kozerke, S., Weber, O. M., Boesiger, P. (2002). Single breath-hold extended free-breathing navigator-gated three- dimensional coronary MRA. *J. Magn. Reson. Imaging* 15:210–214.

Ishikawa, T., Brandt, P. W. (1985). Anomalous origin of the left main coronary artery from the right anterior aortic sinus: angiographic definition of anomalous course. *Am. J. Cardiol.* 55:770–776.

Johnson, L. W., Krone, R. (1993). Cardiac catheterization 1991: a report of the Registry of the Society for Cardiac Angiography and Interventions (SCA&I). *Cathet. Cardiovasc. Diagn.* 28:219–220.

Kawada, N., Sakuma, H., Nomura, Y., Takeda, K. (1998). Value of Breath-hold MR Flow Measurement in Evaluating Stenosis of the Internal Mammary Artery Bypass Graft. *Circulation* 98(Suppl):I-515.

Kerr, A.B., Pauly, J.M., Nishimura, D.G. (1998). Partial k-space acqusiition for real-time MR imaging. Proceedings of the 6th. Anual Meeting of the ISMRM, Sydney, Australia, 1945

Kessler, W., Achenbach, S., Moshage, W., Zink, D., Kroeker, R., Nitz, W., Laub, G., Bachmann, K. (1997). Usefulness of respiratory gated magnetic resonance coronary angiography in assessing narrowings > or = 50% in diameter in native coronary arteries and in aortocoronary bypass conduits. *Am. J. Cardiol.* 80:989–993.

Kessler, W., Laub, G., Achenbach, S., Ropers, D., Moshage, W., Daniel, W. G. (1999). Coronary arteries: MR angiography with fast contrast-enhanced three-dimensional breath-hold imaging–initial experience. *Radiology* 210:566–572.

Kim, W. Y., Danias, P. G., Stuber, M., Flamm, S. D., Plein, S., Nagel, E., Langerak, S. E., Weber, O. M., Pedersen, E. M., Schmidt, M., Botnar, R. M., Manning, W. J. (2001). Coronary magnetic resonance angiography for the detection of coronary stenoses. *N. Engl. J. Med.* 345:1863–1869.

Kimbiris, D., Iskandrian, A. S., Segal, B. L., Bemis, C. E. (1978). Anomalous aortic origin of coronary arteries. *Circulation* 58:606–615.

Krone, R. J., Johnson, L., Noto, T. (1996). Five year trends in cardiac catheterization: a report from the Registry of the Society for Cardiac Angiography and Interventions. *Cathet. Cardiovasc. Diagn.* 39:31–35.

Kurihara, Y., Yakushiji, Y. Y., Tani I, Nakajima, Y., van Cauteren M. (2001). Sensitivity Encoding (SENSE): advantages and disadvantages. Proceedings of the International Society of Magnetic Resonace in Medicine 2001, Glasgow, UK, April 21–27, 1802.

Langerak, S. E., Kunz, P., Vliegen, H. W., Lamb, H. J., Jukema, J. W., van der Wall, E. E., de Roos, A., Improved, M. R. (2001). flow mapping in coronary artery bypass grafts during adenosine-induced stress. *Radiology* 218:540–547.

Langerak, S. E., Vliegen, H. W., de Roos, A., Zwinderman, A. H., Jukema, J. W., Kunz, P., Lamb, H. J., Der Wall, E. E. (2002). Detection of vein graft disease using high-resolution magnetic resonance angiography. *Circulation* 105:328–333.

Lewis, R. P., Rittogers, S. E., Froester, W. F., Boudoulas, H. (1977). A critical review of the systolic time intervals. *Circulation* 56:146–158.

Li, D., Dolan, R. P., Walovitch, R. C., Lauffer, R. B., Three-dimensional, M. R. I. (1998). of coronary arteries using an intravascular contrast agent. *Magn. Reson. Med.* 39:1014–1018.

Li, D., Zheng, J., Weinmann, H. J. (2001). Contrast-enhanced M.R.imaging of coronary arteries: comparison of intra- and extravascular contrast agents in swine. *Radiology* 218:670–678.

Li, D., Carr, J. C., Shea, S. M., Zheng, J., Deshpande, V. S., Wielopolski, P. A., Finn, J. P. (2001). Coronary arteries: magnetization-prepared contrast-enhanced three- dimensional volume-targeted breath-hold MR angiography. *Radiology* 219:270–277.

Manning, W. J., Li, W., Edelman, R. R. (1993). A preliminary report comparing magnetic resonance coronary angiography with conventional angiography. *N. Engl. J. Med.* 328:828–832.

McCarthy, R., Deshpande, V. S., Shea, S. M., Finn, J. P., Li, D. (2001). 3D Magnetization-prepared true-FISP: initial clinical evaluation of a new MR technique for imgaing coronary arteries. *Radiology* 221(supplement):588, RSNA 87th Scientific Assembly and Annual Meeting, Chicago, USA, Nov 25-30, 2001.

McConnell, M. V., Stuber, M., Manning, W. J. (2000). Clinical role of coronary magnetic resonance angiography in the diagnosis of anomalous coronary arteries. *J. Cardiovasc. Magn. Reson.* 2:217–224.

McKinnon, G. C. (1993). Ultrafast interleaved gradient-echo-planar imaging on a standard scanner. *Magn. Reson. Med.* 30:609–616.

Meyer, C. H., Hu, B. S., Nishimura, D. G., Macovski, A. (1992). Fast spiral coronary artery imaging. *Magn. Reson. Med.* 28:202–213.

Misselwitz, B., Schmitt-Willich, H., Ebert, W., Frenzel, T., Weinmann, H. J. (2001). Pharmacokinetics of Gadomer-17, a new dendritic magnetic resonance contrast agent. *MAGMA* 12:128–134.

Molinari, G., Sardanelli, F., Zandrino, F., Balbi, M., Masperone, M. A. (2000). Value of navigator echo magnetic resonance angiography in detecting occlusion/-patency of arterial and venous, single and sequential coronary bypass grafts. *Int. J. Card. Imaging* 16:149–160.

Nitatori, T., Yoshino, H., Yokoyama, K., Hachiya, J., Ishikawa, K. (1999). Coronary M.R. angiography-a clinical experience in Japan. *J. Magn. Reson. Imaging* 10:709–712.

Oppelt, A., Graumann, R., Barfuss, H., Fischer, H., Hartl, W., Shajor, A. (1986). FISP-a new fast MRI sequence. *Electromedica* 54:15–18.

Panych, L. P., Jakab, P. D., Jolesz, F. A. (1993). Implementation of wavelet-encoded MR imaging. *J. Magn. Reson. Imaging* 3:649–655.

Pennell, D. J., Bogren, H. G., Keegan, J., Firmin, D. N., Underwood, S. R. (1996). Assessment of coronary artery stenosis by magnetic resonance imaging. *Heart* 75:127–133.

Plein, S., Bloomer, T. N., Ridgway, J. P., Jones, T. R., Bainbridge, G. J., Sivananthan, M. U. (2001). Steady-state free precession magnetic resonance imaging of the heart: comparison with segmented k-space gradient-echo imaging. *J. Magn. Reson. Imaging* 14:230–236.

Port, M., Corot, C., Raynal, I., Idee, J. M., Dencausse, A., Lancelot, E., Meyer, D., Bonnemain, B., Lautrou, J. (2001). Physicochemical and biological evaluation of p792, a rapid-clearance blood-pool agent for magnetic resonance imaging. *Invest. Radiol.* 36:445–454.

Post, J. C., van Rossum, A. C., Bronzwaer, J. G., de Cock, C. C., Hofman, M. B., Valk, J., Visser, C. A. (1995). Magnetic resonance angiography of anomalous coronary arteries a new gold standard for delineating the proximal course? *Circulation* 92:3163–3171.

Post, J. C., van Rossum, A. C., Hofman, M. B., de Cock, C. C., Valk, J., Visser, C. A. (1997). Clinical utility of two-dimensional magnetic resonance angiography in detecting coronary artery disease. *Eur. Heart J.* 18:426–433.

Pruessmann, K. P., Weiger, M., Scheidegger, M. B., Boesiger, P. (1999). SENSE: sensitivity encoding for fast MRI. *Magn. Reson. Med.* 42:952–962.

Pruessmann, K. P., Weiger, M., Boesiger, P. (2001). Sensitivity encoded cardiac MRI. *J. Cardiovasc. Magn Reson.* 3:1–9.

Redington, R. W., Dumoulin, C. L., Schenck, J. F., Roemer, P. B., Souza, S. P., Mueller, O. M., Eisner, D. R., Piel, J. E., Edelstein, W. A. (1988). MR imaging and bioeffects on a whole body 4.0 Tesla imaging system. *Book of abstracts, Society of Magnetic Resonance in Medicine*. 1. Berkeley, CA: Society of Magnetic Resonance in Medicine, 4.

Regenfus, M., Ropers, D., Achenbach, S., Kessler, W., Laub, G., Daniel, W. G., Moshage, W. (2000). Noninvasive detection of coronary artery stenosis using contrast-enhanced three-dimensional breath-hold magnetic resonance coronary angiography. *J. Am. Coll. Cardiol.* 36:44–50.

Riederer, S. J., Tasciyan, T., Farzaneh, F., Lee, J. N., Wright, R. C., Herfkens, R. J. (1988). MR fluoroscopy: technical feasibility. *Magn. Reson. Med.* 8:1–15.

Rinck, P. A. (1993). *Magnetic Resonance in Medicine*. 3rd ed. London: Blackwell Scientific Publications, pp. 111–142.

Rubinstein, R. I., Askenase, A. D., Thickman, D., Feldman, M. S., Agarwal, J. B., Helfant, R. H. (1987). Magnetic resonance imaging to evaluate patency of aortocoronary bypass grafts. *Circulation* 76:786–791.

Ruehm, S. G., Corot, C., Vogt, P., Kolb, S., Debatin, J. F. (2001). Magnetic resonance imaging of atherosclerotic plaque with ultrasmall superparamagnetic particles of iron oxide in hyperlipidemic rabbits. *Circulation* 103:415–422.

Rzedzian, R. R., Pykett, I. L. (1987). Instant images of the human heart using a new, whole-body MR imaging system. *AJR Am. J. Roentgenol.* 149:245–250.

Saeed, M., Wendland, M. F., Higgins, C. B. (2000). Blood pool MR contrast agents for cardiovascular imaging. *J. Magn. Reson. Imaging* 12:890–898.

Saini, S., Stark, D. D., Rzedzian, R. R., Pykett, I. L., Rummeny, E., Hahn, P. F., Wittenberg, J., Ferrucci, J. T., Forty-millisecond, M. R. (1989). imaging of the abdomen at 2.0 T. *Radiology* 173:111–116.

Sandstede, J. J., Pabst, T., Beer, M., Geis, N., Kenn, W., Neubauer, S., Hahn, D. (1999). Three-dimensional M.R. coronary angiography using the navigator technique compared with conventional coronary angiography. *Am. J. Roentgenol.* 172:135–139.

Sardanelli, F., Molinari, G., Zandrino, F., Balbi, M. (2000). Three-dimensional, navigator-echo MR coronary angiography in detecting stenoses of the major epicardial vessels, with conventional coronary angiography as the standard of reference. *Radiology* 214:808–814.

Scanlon, P. J., Faxon, D. P., Audet, A. M., Carabello, B., Dehmer, G. J., Eagle, K. A., Legako, R. D., Leon, D. F., Murray, J. A., Nissen, S. E., Pepine, C. J., Watson, R. M., Ritchie, J. L., Gibbons, R. J., Cheitlin, M. D., Gardner, T. J., Garson, A. Jr., Russell, R. O. Jr., Ryan, T. J., Smith, S. C. Jr. (1999). ACC/AHA guidelines for coronary angiography. A report of the American College of Cardiology/American Heart Association Task Force on practice guidelines (Committee on Coronary Angiography). *J. Am. Coll. Cardiol.* 33:1756–1824.

Schmermund, A., Rensing, B. J., Sheedy, P. F., Bell, M. R., Rumberger, J. A. (1998). Intravenous electron-beam computed tomographic coronary angiography for segmental analysis of coronary artery stenoses. *J. Am. Coll. Cardiol.* 31:1547–1554.

Serota, H., Barth, C. W., Seuc, C. A., Vandormael, M., Aguirre, F., Kern, M. J. (1990). Rapid identification of the course of anomalous coronary arteries in adults: the "dot and eye" method. *Am. J. Cardiol.* 65:891–898.

Shea, S. M., Deshpande, V. S., Chung, Y., Finn, J. P., Li, D. (2002). 3D True-FISP imaging of the coronary artries: improved contrast with T2-preparation. The society for cardiovascular magnetic resonance. *J. Cardiovasc. Magn. Reson.* #236:26, Fifth Annual Scientific Sessions, Florida, USA, Jan 25-27.

Sodickson, D. K., Griswold, M. A., Jakob, P. M. (1999). SMASH imaging. *Magn. Reson. Imaging Clin. N. Am.* 7:237–254.

Spuentrup, E., Ruebben, A., Schaeffer, T., Günther, R. W., Buecker, A. (2002). MR-Guided Coronary artery stent placement in a pig model using interactive real-time balanced FFE. Society for Cardiovascular Magnetic Resonance. *J. Cardiovasc. Magn. Reson.* 4(1):147, Fifth Annual Scientific Sessions, Florida, USA, Jan 25-27.

Spuentrup, E., Manning, W. J., Botnar, R. M., Kissinger, K. V., Stuber, M. (2002). Impact of navigator timing on free-breathing submillimeter 3D coronary magnetic resonance angiography. *Magn. Reson. Med.* 47:196–201.

Staffeld, H. F., Mertens, H. M., Gleichmann, U. (1978). Influence of dynamic exercise and training on systolic time intervals in normals and patients with coronary heart disease (author's transl). *Z. Kardiol.* 67:305–316.

Steenbeck, J., Pruessmann, K. (2001). Technical developments in cardiac MRI: 2000 update. *Rays* 26:15–34.

Stuber, M., Scheidegger, M.B., Boesiger, P. (1997). Realtime Imaging of the Heart. Proceedings of the 5th. Anual Meeting of the ISMRM, Vancouver, Canada, 908

Stuber, M., Botnar, R. M., Danias, P. G., McConnell, M. V., Kissinger, K. V., Yucel, E. K., Manning, W. J. (1999). Contrast agent-enhanced, free-breathing, three-dimensional coronary magnetic resonance angiography. *J. Magn. Reson. Imaging* 10:790–799.

Stuber, M., Botnar, R. M., Danias, P. G., Kissinger, K. V., Manning, W. J. (1999). Submillimeter three-dimensional coronary MR angiography with real-time navigator correction: comparison of navigator locations. *Radiology* 212:579–587.

Stuber, M., Botnar, R. M., Spuentrup, E., Kissinger, K. V., Manning, W. J. (2001a). Three-dimensional high-resolution fast spin-echo coronary magnetic resonance angiography. *Magn. Reson. Med.* 45:206–211.

Stuber, M., Botnar, R. M., Kissinger, K. V., Manning, W. J. (2001b). Free-breathing black-blood coronary MR angiography: initial results. *Radiology* 219:278–283.

Stuber, M., Botnar, R.M., Lamerichs, R., Fischer, S.E., Smink, J., Harvey, P.R., Manning, W.J. (2002). A Preliminary Report on In-Vivo Coronary MRA at 3 Tesla in Humans. ISMRM Tenth Scientific Meeting & Exhibition, Honolulu, Hawaii, May 18–24, #0116

Taylor, A. M., Panting, J. R., Keegan, J., Gatehouse, P. D., Amin, D., Jhooti, P., Yang, G. Z., McGill, S., Burman,

E. D., Francis, J. M., Firmin, D. N., Pennell, D. J. (1999). Safety and preliminary findings with the intravascular contrast agent NC100150 injection for MR coronary angiography. *J. Magn. Reson. Imaging* 9:220–227.

Taylor, A. M., Thorne, S. A., Rubens, M. B., Jhooti, P., Keegan, J., Gatehouse, P. D., Wiesmann, F., Grothues, F., Somerville, J., Pennell, D. J. (2000). Coronary artery imaging in grown up congenital heart disease: complementary role of magnetic resonance and x-ray coronary angiography. *Circulation* 101:1670–1678.

Thiele, H., Nagel, E., Paetsch, I., Schnackenburg, B., Bornstedt, A., Kouwenhoven, M., Wahl, A., Schuler, G., Fleck, E. (2001). Functional cardiac MR imaging with steady-state free precession (SSFP) significantly improves endocardial border delineation without contrast agents. *J. Magn. Reson. Imaging* 14:362–367.

Toussaint, J. F., LaMuraglia, G. M., Southern, J. F., Fuster, V., Kantor, H. L. (1996). Magnetic resonance images lipid, fibrous, calcified, hemorrhagic, and thrombotic components of human atherosclerosis in vivo. *Circulation* 94:932–938.

Vliegen, H. W., Doornbos, J., de Roos, A., Jukema, J. W., Bekedam, M. A., van der Wall, E. E. (1997). Value of fast gradient echo magnetic resonance angiography as an adjunct to coronary arteriography in detecting and confirming the course of clinically significant coronary artery anomalies. *Am. J. Cardiol.* 79:773–776.

Vrachliotis, T. G., Bis, K. G., Aliabadi, D., Shetty, A. N., Safian, R., Simonetti, O. (1997). Contrast-enhanced breath-hold MR angiography for evaluating patency of coronary artery bypass grafts. *AJR Am. J. Roentgenol.* 168:1073–1080.

Wang, Y., Riederer, S. J., Ehman, R. L. (1995). Respiratory motion of the heart: kinematics and the implications for the spatial resolution in coronary imaging. *Magn. Reson. Med.* 33:713–719.

Wang, Y., Vidan, E., Bergman, G. W. (1999). Cardiac motion of coronary arteries: variability in the rest period and implications for coronary MR angiography. *Radiology* 213:751–758.

Wang, Y., Watts, R., Mitchell, I., Nguyen, T. D., Bezanson, J. W., Bergman, G. W., Prince, M. R. (2001). Coronary M.R. angiography: selection of acquisition window of minimal cardiac motion with electrocardiography-triggered navigator cardiac motion prescanning–initial results. *Radiology* 218:580–585.

Weber, C., Steiner, P., Sinkus, R., Dill, T., Bornert, P., Adam, G. (2002). Correlation of 3D MR coronary angiography with selective coronary angiography: feasibility of the motion-adapted gating technique. *Eur. Radiol.* 12:718–726.

Weiger, M., Börnert, P., Proksa, R., Schaffter, T., Haase, A. (1997). Motion-adapted gating based on k-space weighting for reduction of respiratory motion artifacts. *Magn. Reson. Med.* 38:322–333.

Weiger, M., Pruessmann, K. P., Boesiger, P. (2000). Cardiac real-time imaging using SENSE SENSitivity Encoding scheme. *Magn. Reson. Med.* 43:177–184.

Weissler, A. M., Harris, W. S., Schoenfeld, C. D. (1968). Systolic time intervals in heart failure in man. *Circulation* 37:149–159.

Wen, H., Denison, T. J., Singerman, R. W., Balaban, R. S. (1997). The intrinsic signal-to-noise ratio in human cardiac imaging at 1.5, 3, and 4 T. *J. Magn. Reson.* 125:65–71.

White, R. D., Caputo, G. R., Mark, A. S., Modin, G. W., Higgins, C. B. (1987). Coronary artery bypass graft patency: noninvasive evaluation with MR imaging. *Radiology* 164:681–686.

White, R. D., Pflugfelder, P. W., Lipton, M. J., Higgins, C. B. (1988). Coronary artery bypass grafts: evaluation of patency with cine MR imaging. *AJR Am. J. Roentgenol.* 150:1271–1274.

Wielopolski, P. A., van Geuns, R. J., de Feyter, P. J., Oudkerk, M. (1998). Breath-hold coronary MR angiography with volume-targeted imaging. *Radiology* 209:209–219.

Wintersperger, B. J., Engelmann, M. G., von Smekal, A., Knez, A., Penzkofer, H. V., Hofling, B., Laub, G., Reiser, M. F. (1998). Patency of coronary bypass grafts: assessment with breath-hold contrast-enhanced MR angiography-value of a non-electrocardiographically triggered technique. *Radiology* 208:345–351.

Woodard, P. K., Li, D., Haacke, E. M., Dhawale, P. J., Kaushikkar, S., Barzilai, B., Braverman, A. C., Ludbrook, P. A., Weiss, A. N., Brown, J. J., Mirowitz, S. A., Pilgram, T. K., Gutierrez, F. R. (1998). Detection of coronary stenoses on source and projection images using three-dimensional MR angiography with retrospective respiratory gating: preliminary experience. *Am. J. Roentgenol.* 170:883–888.

van Geuns, R. J., Wielopolski, P. A., de Bruin, H. G., Rensing, B. J., Hulshoff, M., van Ooijen, P. M., de Feyter, P. J., Oudkerk, M. (2000). MR coronary angiography with breath-hold targeted volumes: preliminary clinical results. *Radiology* 217:270–277.